JOURNAL OF MAGNETIC RESONANCE **133,** 13–20 (1998)
ARTICLE NO. MN981439

Pulse Sequences for Steady-State Saturation of Flowing Spins

Ian Marshall

Department of Medical Physics and Medical Engineering, University of Edinburgh, Edinburgh, United Kingdom

Received September 5, 1997; revised January 6, 1998

It is useful to be able to suppress the NMR signal from spins in a flowing fluid, for example for ''black-blood'' visualization of blood vessels *in vivo,* **for the suppression of flow artifacts, and for the estimation of tissue perfusion by continuous labeling of inflowing arterial spins. This work considers the flow of fluid through a region in which it is subjected to a train of saturation pulses. Computer simulations and** *in vitro* **measurements show that a train of equal-duration spoiler pulses produces less effective suppression than does a train of pulses of geometrically increasing duration. It is shown analytically that a long train of ideal equal-duration spoiler pulses converts initial magnetization (0, 0, M_0) into a combination of longitudinal and transverse magnetization equal to 0.29 ($-M_0$, 0, M_0) and is therefore unsatisfactory for continuous saturation.**

INTRODUCTION

Calculation of the NMR signal strength from flowing spins is a complex problem that has been treated mathematically for both spin echo (*1*) and gradient echo (*2*) sequences. In magnetic resonance imaging (MRI) one may wish to retain the signal from spins in flowing fluids, and there is a large literature on methods to achieve this (*3–6*). In the medical field, the imaging of spins in flowing blood is termed angiography and allows the *in vivo* visualization of blood flow in the major arteries and veins (*5–7*). However, in this work we are concerned with the opposite problem, that of deliberately suppressing the signal from flowing spins. Such a technique is useful for reducing flow-related artifacts (*8*), for ''black-blood'' angiography (*9*), and for the estimation of tissue blood perfusion (*10–14*). In the last application, arterial blood is magnetically labeled or ''tagged.'' Subtraction of labeled images from nonlabeled images then yields perfusion images that may be quantified using longitudinal relaxation (T1) maps. Steady-state labeling of inflowing arterial blood may be achieved either by saturation (*11, 13, 14*) or by inversion (*10, 12*). Although spin inversion theoretically gives twice as much signal as saturation, it requires the delivery of continuous radio frequency (RF) energy to effect adiabatic fast passage (*15*), and is therefore difficult to implement on standard scanners which normally allow only pulsed RF. Pulsed labeling techniques (*16–18*) are gaining in popularity, but yield lower intrinsic signal-to-noise ratios than their continuous counterparts and are more difficult to quantify. In this work, we investigated the design of gradient pulse trains for the continuous saturation of flowing fluid.

Continuous saturation is achieved by using an imaging sequence with relatively long repetition time (TR), and filling most of TR with saturation pulses (*11, 13, 14*). The actual imaging part of the sequence is kept short to maximize the saturation efficiency. The imaging readout may be achieved by echo-planar (single- or multishot) or by conventional spin echo techniques. Each ''saturation'' pulse consists of a 90° RF pulse to excite the spins, followed by a gradient spoiler pulse to dephase the transverse magnetization. Multiple pulses are required to ensure that all the blood magnetization passing through the saturation region is spoiled, regardless of its flow velocity. Slow flowing blood will have been exposed to several saturation pulses, and possibly more than one repetition of the entire saturation/imaging sequence. On the other hand, fast flowing blood will have experienced only one or a few saturation pulses, and the maximum flow velocity determines the maximum allowable spoiler pulse duration. The simplest implementation uses spoiler pulses of equal duration (*8, 11*). However, this is unsatisfactory because of the unwanted refocusing of magnetization (production of stimulated echoes) in blood that is flowing slowly enough to experience three or more pulses. This occurs because gradient spoiling is a reversible, coherent process (*19, 20*), and care is therefore required in the design of multiple pulse trains. Barker and Mareci (*20*) show that to avoid stimulated echoes the time integrals of successive spoiler pulses should be related geometrically.

In this work, we conducted computer simulations and *in vitro* measurements of constant amplitude saturation pulse trains having (a) equal-duration pulses and (b) geometrically increasing pulse durations in order to assess the effectiveness of continuous saturation of flowing fluid. Our goal was the suppression of flowing fluid regardless of its velocity and regardless of the subsequent imaging technique, so we concentrate on what happens in the saturation region.

1090-7807/98 $25.00

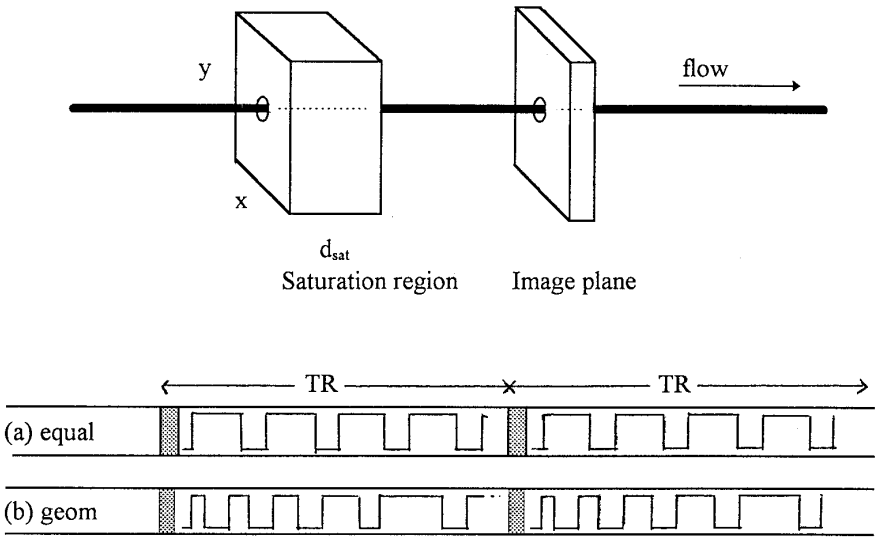

FIG. 1. Schematic diagram showing blood flowing through a saturation region of thickness d_{sat} prior to an imaging plane. The sequence repetition time TR is filled with either (a) equal-duration or (b) geometrically increasing duration spoiler gradient pulses, with each spoiler pulse being preceded by a 90° RF excitation pulse. The blood experiences a number of spoiler pulses depending on its velocity, with slow flowing blood experiencing more than one complete train of pulses during its transit of the saturation region. The shaded areas represent the imaging periods in between successive saturation pulse trains.

METHOD

Simulations

Simulations were conducted on a Sun UltraSparc computer (Sun Microcomputers, Mountain View, CA) and were written in C. Visualization of results was implemented using Matlab (The Mathworks, Natick, MA). Blood of velocity v travels in the z-direction through a region of thickness d_{sat} in which it is exposed to a train of saturation pulses (Fig. 1). Each saturation pulse was modeled as a combination of a 90° RF pulse followed by a spoiler gradient pulse that causes a dephasing of transverse magnetization. The spoiler pulses had durations $T_{spoil(i)}$ and intervals $T_{gap(i)}$, where $i = 1, 2, \ldots, n$, and where n is the number of spoiler pulses in the train. The spoiler pulse train is followed by the imaging period T_{im}. Blood traveling faster than $v = d_{sat}/(T_{spoil(n)} + T_{gap(n)})$ experiences no excitation pulses, and will therefore be unaffected.

A simplified form of the Bloch equations was used, in which all operations (RF pulses, spoiling, and simple relaxation) were represented by matrix rotations of the magnetization $\mathbf{M} = (M_x, M_y, M_z)$. The pulse sequence is thus reduced to a succession of matrix multiplications. RF pulses were regarded as acting instantaneously to produce a 90° rotation of the magnetization about the y-axis.

Each (x, y) pixel in the downstream image plane contains spins that have passed through a corresponding position in the saturation region. In the first part of the Appendix, it is explained how spoiling was simulated by summing the contribution of spin isochromats across the pixel in the direction of the applied spoiling gradient. The readout (x) direction was chosen for spoiling. The number of isochromats was adjusted automatically to satisfy Eq. [4] (Appendix), and we used a calculation time step of 100 μs. The computation time is proportional to the number of time steps and to the number of isochromats, and therefore increases as the square of the transit time across the saturation region. We used relaxation times of T1 = 2 s and T2 = 1 s to represent water, and T1 = 1 s and T2 = 250 ms to represent blood (*21*). The saturation region thickness was 30 mm, and the image pixel size was 1 mm. Fluid velocities from 0.01 to 1.00 m/s (in steps of 0.01 m/s) were studied, covering the range of blood velocities encountered *in vivo*. Two spoiler pulse trains were studied: one with nine pulses of equal duration (8.8 ms), and the other with nine pulses whose durations increased geometrically by a factor of 1.5 (1.1, 1.6, 2.4, . . . , 12, 18, 27 ms). The spoiler pulse amplitude was 10 mT/m. The gap between all spoiler pulses was 4.4 ms, this being the time taken for slice selection and selective RF excitation available on our scanner. To study the effects of the saturation sequence itself, the interval between repetitions of the spoiler train (the imaging period T_{im}) was set to zero. The final magnetization of the blood (as it exits the saturation region) was saved in text files as a function of velocity.

In Vitro Flow Experiment

Imaging was carried out on a Siemens 1.5-T Magnetom 63SP (Siemens Medical, Erlangen, Germany) equipped with unshielded 10 mT/m gradients having a maximum slew rate of 10 T/m/s. The standard head coil was used.

A flow phantom was constructed from rigid plastic tubing (bore 6.1 mm) immersed in a water bath. The phantom was fed tap water from a constant pressure-head upper reservoir and

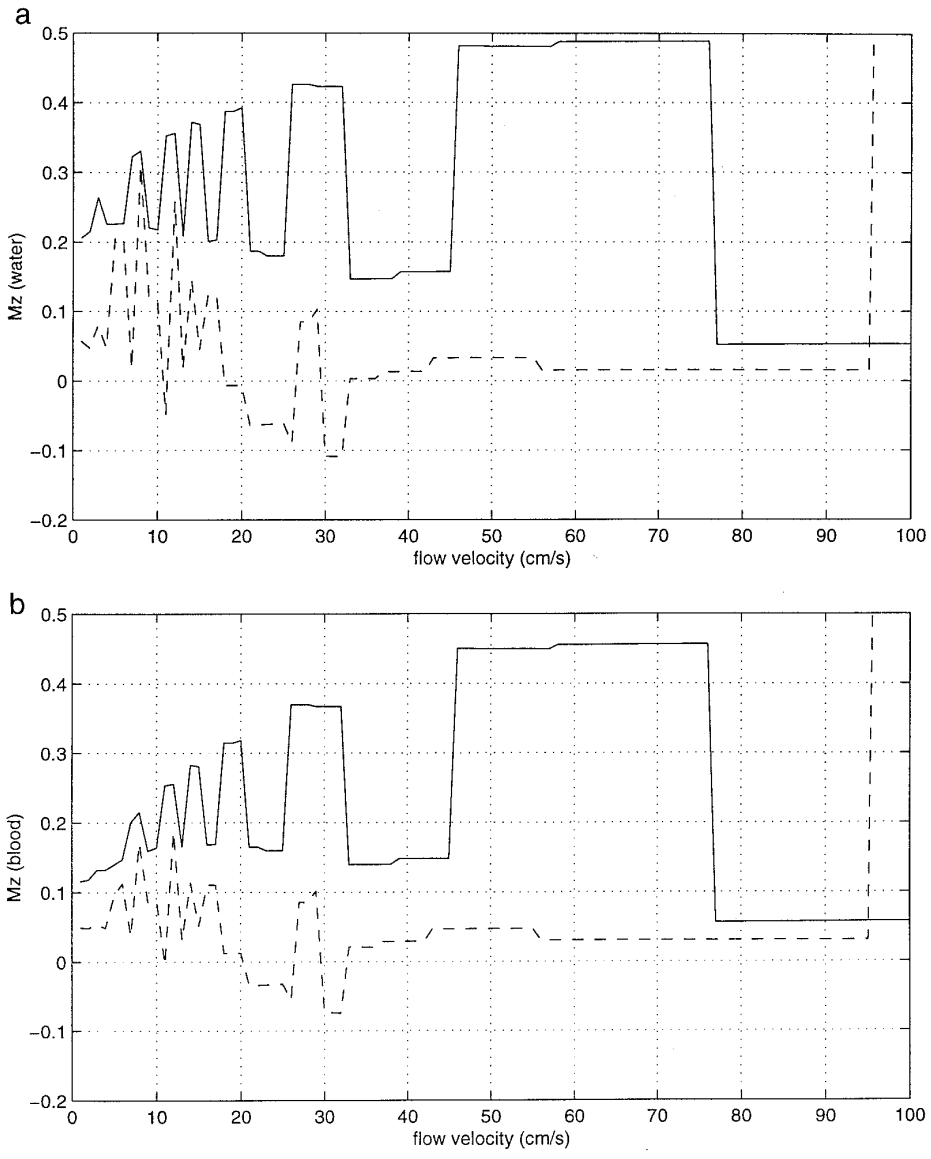

FIG. 2. Theoretical residual longitudinal magnetization M_z as a function of flow velocity, for spoiler pulses of equal duration (solid line) and geometrically increasing duration (dashed line). (a) Water with T1 = 2 s and T2 = 1 s; (b) blood with T1 = 1 s and T2 = 250 ms. See text for details of sequence timing.

was drained to a lower reservoir via a flow control valve. A peristaltic pump (type 302S, Watson-Marlow, Falmouth, UK) recirculated the water to the upper reservoir. Imaging measurements were made at a flow rate of 620 ml/min (determined by timed collection of water), corresponding to a mean flow velocity of 35 cm/s.

A spin-echo sequence (echo time TE = 25 ms) was modified to incorporate a train of nine saturation pulses acting on a single, user-defined saturation region. Each saturation pulse consisted of a 90° RF pulse followed by a gradient spoiling pulse of 10 mT/m amplitude. In one variant all the spoiler pulses had a duration of 8.8 ms, whereas in a second sequence pulses with geometrically increasing spoiler durations (factor 1.5) were implemented (as described previously). All spoiler pulses were applied in the readout (x) direction. The total TR of the sequence was 168 ms.

Images in a plane perpendicular to the flow direction were acquired with a 256-mm field of view (FOV), with a 30-mm thick parallel saturation region positioned either upstream or downstream of the region of interest. The separation between the centers of the image and saturation planes was 80 mm, at which distance direct interaction was negligible. An image plane thickness of 15 mm was used to minimize spin washout effects (*8*). Other imaging parameters were 256 × 256 matrix (i.e., 1 mm pixel dimensions) and four acquisitions. Both the equal-duration and geometric saturation sequences were used.

Phase-contrast velocity mapping images were also collected in the same image plane.

TABLE 1

Theoretical Value of Longitudinal Magnetization M_z Remaining after Application of a Number of Ideal Equal-Duration Spoiler Pulses

Number of pulses n	M_z	M_z
1	0	0.000
2	0	0.000
3	1/2	0.500
4	1/2	0.500
5	1/8	0.125
6	1/8	0.125
7	7/16	0.438
8	7/16	0.438
9	21/128	0.164
10	21/128	0.164

Note. Both exact and decimal values are given (see Appendix).

RESULTS AND DISCUSSION

Simulations

Figure 2 shows the simulated residual longitudinal magnetization M_z (which contributes to the image) for spins which have passed through a saturation region of 30-mm thickness. In the saturation region they experience either the train of equal-duration saturation pulses (solid line) or the train of geometrically increasing spoiler durations (dashed line). Results are shown for T1 and T2 relaxation parameters representative of water (Fig. 2a) and representative of blood (Fig. 2b). The behavior of M_z is similar for the two fluids, with water having the higher residual magnetization and therefore being more difficult to suppress. The behavior of M_z for the equal-duration spoilers is striking, alternating between two values that appear to converge as the velocity decreases (i.e., number of applied pulses increases). In the second part of the Appendix, it is shown how theoretical values of M_z can be calculated for ideal spoiler pulses (complete dephasing) in the absence of relaxation effects. These values are given in Table 1 for the first 10 pulses, corresponding to flow velocities above 20 cm/s.

The simulations for water are in reasonable agreement with these theoretical values, any discrepancies being attributable to the fact that the simulations include the effects of relaxation with T1 = 2s and T2 = 1s, and that for 10 mT/m gradient pulses, dephasing is not quite complete for the simulated 1-mm pixels and spoiler pulses of duration 8.8 ms. In fact, zeroes of the spoiling function (Appendix, Eq. [2]), corresponding to successive complete wraps of the magnetization, occur at multiples of 2.3 ms under these conditions. In between the zeroes, spoiling is dependent on the $1/\omega t$ envelope term.

For velocities between 77 and 100 cm/s, very effective spoiling is achieved with equal-duration spoilers. However, lower velocities lead to three or more pulses being applied to the flowing fluid, and stimulated echoes are generated so that the spoiling is poor; for example, only 50% suppression is (ideally) achieved with three or four pulses (velocities between 46 and 76 cm/s). The lower the flow velocity, the greater the number of spoiler pulses experienced during transit of the saturation band. The residual magnetization oscillates between two extremes that appear to converge slowly as the number of pulses increases (Fig. 2 and Table 1). In the third part of the Appendix, an analytical solution for the case of a very large number of (ideal) equal-duration pulses is given, and it is shown that the longitudinal magnetization tends towards a value of $[1 - (\sqrt{2}/2)]M_0 = 0.29\,M_0$.

Figure 2 (dashed line) shows the residual M_z for the train of nine spoiler pulses of amplitude 10 mT/m and with geometrically increasing durations. For velocities above 95 cm/s, the transit time is less than the duration of the last spoiler pulse and gap ((27 + 4.4) ms), so that the fluid is not excited at all, and hence no spoiling occurs. For velocities in the range 33 to 95 cm/s, excellent spoiling is achieved, as stimulated echoes are avoided by the use of increasing spoiler pulse durations which prevent the refocusing of magnetization. For velocities in the range 21 to 32 cm/s, the spoiling is not quite so good (residual $|M_z|$ around 0.1) as the fluid has experienced the shortest spoiler pulses which are inadequate to cause complete dephasing. For velocities below 21 cm/s, more than one complete train of pulses is experienced during transit, and the spoiling efficiency is not maintained as stimulated echoes are again produced.

Flow Experiment

Figure 3 shows the results of the *in vitro* flow phantom experiment. The theoretical value for the Reynolds number is 1940 for the 620 ml/min flow rate, and conditions should therefore be nonturbulent. We also took care to provide a long straight inlet length (approximately 80 cm) to allow the flow to become fully developed before entering the imaging region. Conditions of laminar flow were confirmed by the parabolic velocity profile obtained from the phase-contrast images.

In the absence of upstream saturation (Fig. 3a), the inflowing water appears bright in comparison with the surrounding water bath (inflow enhancement effect). There is no signal from the tube walls. The central pixels have a reduced intensity because the flow velocity there is great enough for spins to pass completely through the image slice in the echo time between excitation and imaging (washout effect). Assuming laminar flow, the peak velocity in our experiment was 70 cm/s (twice the mean velocity), whereas fluid traveling at greater than 60 cm/s will wash out of the 15-mm thick imaging slice during the 25-ms echo time. We therefore discarded the central pixels in the subsequent analysis. Other pixels will exhibit varying degrees of signal loss due to washout, but the effect will be the same regardless of the saturation sequence used, so that a direct comparison is possible. Fluid near the vessel walls also has a reduced intensity, presumably because the greater radial veloc-

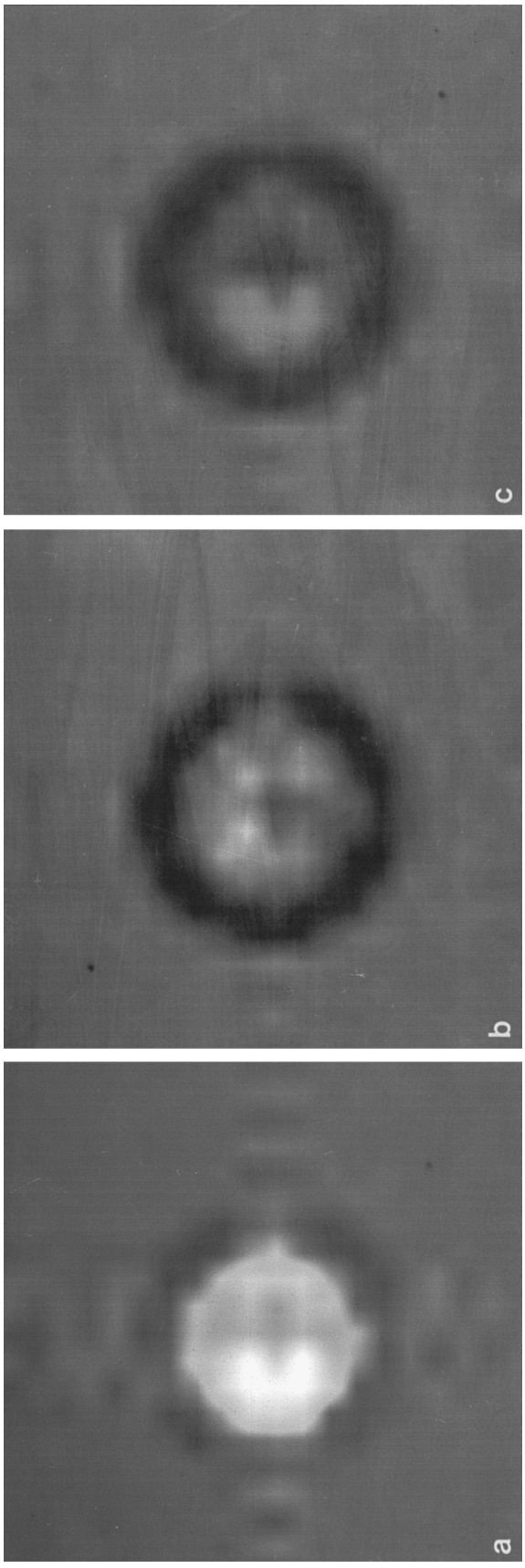

FIG. 3. *In vitro* spin-echo images, acquired perpendicular to the direction of flow. The mean flow velocity was 35 cm/s. (a) 30-mm saturation region positioned 80 mm downstream of image plane; (b) 30-mm saturation band with equal-duration spoiler gradient pulses positioned 80 mm upstream of image plane; (c) 30-mm saturation band with geometrically increasing spoiler gradient durations positioned 80 mm upstream of image plane. The windowing is the same for all three images.

ity gradient there leads to dephasing of the spins within a pixel. We did not use flow-compensated sequences in this work, as we wished to study the saturation effects in isolation. Some ghosting is apparent in the phase (vertical) direction, and Fourier ringing (Gibbs artifact) can be observed in the readout (horizontal) direction.

When the saturation band is moved upstream of the image plane, the flowing fluid signal intensity is reduced (Figs. 3b and 3c). Signal intensity measurements were made on an annular region of interest (ROI) of outer radius 3 mm (coinciding with the tube wall) and inner radius 1 mm to exclude fluid that theoretically exhibits complete washout. Suppression factors of 5.0 (i.e., residual $M_z = 0.20$) and 6.5 ($M_z = 0.15$) were found for the equal-duration and geometric saturation sequences, respectively.

It is possible to calculate the residual M_z expected from the ROI by using the radial velocity distribution and the results of Fig. 2a. At each radius (1–3 mm, in sufficiently small steps), the velocity is calculated assuming a parabolic profile with a central maximum velocity of 70 cm/s. M_z for that velocity is read from the data file corresponding to Fig. 2a, and the signal is multiplied by the elemental annular area. These contributions are summed over the range of radii corresponding to the annular ROI. The resulting theoretical suppression factors (residual M_z) for the equal-duration and the geometrically increasing duration spoiler pulse trains are 3.6 (0.28) and 36 (0.03), respectively.

Thus, the experimental suppression factor of 5.0 for the equal-duration sequence is rather better than the 3.6 expected from the simulations, whereas the factor of 6.5 for the geometrical sequence is rather disappointing compared with the theoretical value of 36. Nonetheless, the geometric sequence yields a modest but worthwhile improvement over the equal-duration sequence under these conditions.

The poor performance of the geometric sequence (relative to the simulations) may be due to several factors. We did not model the effect of the imaging sequence itself in the simulations presented here. Although the image readout gradient (applied in the same (x) direction as the spoiler gradient) will perturb the carefully balanced timing of the geometrical pulse train, thereby causing some unwanted refocusing of magnetization, preliminary results from more complete simulations suggest that the effect may not be very significant. Another simplification made in the simulations was that the RF pulses were regarded as acting instantaneously. In the actual sequences, their duration was 2.56 ms, during which time spins will move slightly, thus complicating the excitation profile. Slice select gradient pulses are applied (in the direction of flow) simultaneously with the RF pulses in order to define the saturation region. The effects of these pulses are extremely complex to evaluate, as ω (Eq. [1], Appendix) itself then becomes a function of time, and the simple model of spoiling no longer holds. However, because these pulses are applied in a direction orthogonal to the spoiler trains, their effect should

be to increase the suppression factor, and this may explain why the equal-duration spoiler sequence performed better than suggested by the corresponding simulation. A further complication is the nonideal saturation band profile, such that spins experiencing an excitation pulse when near either edge of the band will be flipped not by 90° but by some lower angle. Eddy current effects may also contribute to the discrepancies between theory and experiment.

Although fast-flowing fluids with long T1 will not reach equilibrium magnetization in the time available between entering the 1.5-T field of the scanner and reaching the imaging region, this applies equally to both types of spoiler sequence and should not be important so long as a direct comparison is made with all other factors being held the same. Increasing the time the fluid spends in the scanner would entail folding or coiling the inlet tube, thus disrupting the laminar flow. Similarly, relaxation of magnetization between the saturation and image planes will affect both spoiler sequences equally.

Figure 2 suggests that the suppression of signal from blood should be slightly easier than for water, because of the reduced T1 and T2. The experimental study with water therefore represents a worst case, as well as being much more convenient to carry out. Although we did not explicitly study pulsatile flow, we have studied the range of velocities encountered *in vivo* by taking care to make measurements under conditions of laminar flow.

The inadvertent creation of stimulated echoes was not discussed by Mugler and Brookeman (*8*) in their investigation of flow artifact suppression, but can be observed in their results for slow flow where poor suppression is achieved. Unfortunately, they do not give any details of the spoiling pulses used.

Stimulated echoes could be avoided if the spoiler gradients were applied along orthogonal directions for successive repetitions of the pulse sequence, but there will be a lower velocity below which all three orthogonal directions have been used and stimulated echoes then become inevitable. This situation could be avoided by increasing the length of the basic pulse train. This is not a straightforward matter, however, since adding shorter pulses at the beginning of the train does little to increase the overall time, and in any case, they may not be long enough to achieve adequate dephasing. Adding longer pulses at the end of the train leads very quickly to excessive spoiler pulse durations so that the maximum allowable flow velocity is severely reduced. One solution would be to reduce the geometric factor, although this would weaken the overall suppression achieved. The value of 1.5 used in this work is a compromise between the factor 2 suggested by Barker and Mareci (*20*) and lower, less effective values. In continuous suppression schemes, there is a need to balance the pulse durations against the range of velocities likely to be encountered. Since it is the integrated amplitude–time function that determines the amount of dephasing (*19, 20*), it would also be possible to vary the spoiler gradient pulse amplitudes rather than their durations. However, similar limitations apply: Low amplitudes would not produce adequate spoiling, and the available hardware sets an upper limit. An alternative approach is RF dephasing (*22*), which was used by Karlsen *et al.* (*13*) in combination with gradient spoiling.

CONCLUSIONS

The continuous saturation of magnetization in a flowing fluid is a nontrivial problem when a range of velocities is present, as in the *in vivo* case. The use of a train of geometrically increasing duration spoiler gradient pulses leads to more effective suppression than does a train consisting of equal-duration spoilers, since stimulated echoes are avoided. Simulations suggested that the magnetization of water flowing under laminar conditions and with a mean velocity of 35 cm/s could be suppressed by factors of 3.6 and 36 using equal-duration and geometrically increasing duration spoiler pulses, respectively. With a flow phantom, the actual suppression factors achieved were 5.0 and 6.5, respectively. Reasons for the discrepancy, particularly the disappointing performance of the geometric sequence, may include finite-duration RF pulses, saturation region slice select gradients, and imaging gradients. These effects are being studied in more complete simulations.

It is shown analytically that a long train of ideal equal-duration spoiler pulses converts initial magnetization $(0, 0, M_0)$ into a combination of longitudinal and transverse magnetization equal to 0.29 $(-M_0, 0, M_0)$, and is therefore unsatisfactory for continuous saturation.

APPENDIX

Simulation of Spoiling

In between applied RF pulses, the magnetization relaxes with time constants T1 and T2, which are the longitudinal and transverse decay times, respectively. Relaxation over a period τ is represented by the matrix R, where

$$\mathsf{R} = \begin{pmatrix} \exp(-\tau/T2)\cos(\omega\tau) & -\exp(\tau/T2)\sin(\omega\tau) & 0 & 0 \\ \exp(-\tau/T2)\sin(\omega\tau) & \exp(-\tau/T2)\cos(\omega\tau) & 0 & 0 \\ 0 & 0 & 0 & 0 \\ 0 & 0 & \exp(-\tau/T1) & 1 - \exp(-\tau/T1) \end{pmatrix}. \quad [1]$$

R is applied to the augmented magnetization (M_x, M_y, M_z, M_0), where M_0 is the equilibrium longitudinal magnetization and ω is the effective angular frequency. For on-resonance magnetization in the absence of an applied gradient, ω is zero for all the spins contributing to the signal. When a (spoiling) gradient $\mathbf{G}$ is applied, ω takes on the value $\omega(\mathbf{r}) = \gamma\mathbf{G} \cdot \mathbf{r}$ where γ is the gyromagnetic ratio and $\mathbf{r}$ is the position of the contributing spin

within the image plane. Implicit in this relationship is the time independence of $\omega(\mathbf{r})$; that is, the spoiling gradient is not applied in the direction of flow. Contributions arise from all the spins across a pixel, so that we must consider a range of values of $\mathbf{r}$ (*19*). This amounts to considering a range of frequencies $\omega(\mathbf{r})$, and applying the entire pulse sequence to them all, taking the sum at each discrete time point. Analytically, the effect of an ideal spoiler pulse of duration t (neglecting relaxation) is to reduce the net transverse magnetization from unity to

$$\boldsymbol{M}_{ideal,spoiling} = \frac{1}{\omega_m}\int_0^{\omega_m} e^{(-i\omega t)}d\omega = \frac{i}{\omega_m t}\left(e^{(-i\omega_m t)} - 1\right), \quad [2]$$

where ω_m is the maximum frequency $\omega(\mathbf{r_m}) = \gamma\mathbf{G}\cdot\mathbf{r_m}$, corresponding to the far edge of the pixel at position $\mathbf{r_m}$. Equation [2] represents a behavior that is oscillatory with time, and with an envelope that is inversely proportional to time. The first zero occurs when $\omega_m t = 2\pi$ (i.e., $t = 2\pi/\gamma G r_m$) corresponding to one complete wrap of the magnetization phase across the pixel. Numerical simulations use a number N of discrete ''isochromats'' rather than an integral, and Eq. [2] is replaced by the summation

$$\boldsymbol{M}_{num,spoiling} = \frac{1}{N}\sum_{j=0}^{N-1} e^{(-ij\omega_m t/N)} = \frac{1}{N}\left(\frac{1 - e^{(-i\omega_m t)}}{1 - e^{(-i\omega_m t/N)}}\right). \quad [3]$$

The summation of Eq. [3] differs from the integral of Eq. [2], having subsidiary maxima whenever $\omega_m t/N$ is a multiple of 2π. These ''diffraction grating'' maxima are an artifact of using a discrete sum rather than a continuous integral, and must be avoided in simulations of spoiling by using sufficiently many isochromats so that $\omega_m t/N \ll 2\pi$. This translates to

$$N \gg \frac{\gamma G r_m}{2\pi}\sum_{i=l}^{n} T_{spoil(i)}, \quad [4]$$

where r_m represents the pixel size, and the blood velocity is such that it experiences saturation pulses $l, l+1, \ldots, n$ while traversing the saturation region. When Eq. [4] is satisfied, the spurious maxima are effectively shifted to beyond the time frame of interest.

Analysis of a Train of Equal-Duration Spoilers

Repeated pulses. An exact analytical solution is possible for the case of a train of excitation/spoiler pulses of equal duration. A 90° RF pulse applied along the y-axis can be represented by the rotation matrix P_y, where

$$\mathsf{P}_y = \begin{pmatrix} 0 & 0 & 1 \\ 0 & 1 & 0 \\ -1 & 0 & 0 \end{pmatrix}. \quad [5]$$

Similarly, the application of a gradient spoiling pulse causes a rotation $\theta = \gamma\mathbf{G}\cdot\mathbf{r}t$ about the z-axis, where γ is the gyromagnetic constant, $\mathbf{G}$ is the gradient strength, $\mathbf{r}$ the position of the contributing spin, and t is the pulse duration. This rotation can be represented by the matrix R_θ, where

$$\mathsf{R}_\theta = \begin{pmatrix} \cos(\theta) & -\sin(\theta) & 0 \\ \sin(\theta) & \cos(\theta) & 0 \\ 0 & 0 & 1 \end{pmatrix}. \quad [6]$$

The composite excitation and spoiling pulse C is given by the matrix product $\mathsf{C} = \mathsf{R}_\theta\mathsf{P}_y$, namely,

$$\mathsf{C} = \begin{pmatrix} 0 & -\sin(\theta) & \cos(\theta) \\ 0 & \cos(\theta) & \sin(\theta) \\ -1 & 0 & 0 \end{pmatrix}. \quad [7]$$

In the absence of relaxation, the application of n such pulses to initial magnetization $\mathbf{M}_{init} = (0, 0, M_0)$ leads to a final magnetization $\mathbf{M}_{final} = \mathsf{C}^n\mathbf{M}_{init}$. This can be evaluated explicitly in terms of polynomials of $\sin(\theta)$ and $\cos(\theta)$. Assuming perfect spoiling, all values of θ are equally likely, so that one takes the average over θ. Terms in the polynomials involving odd powers of $\sin(\theta)$ or $\cos(\theta)$ therefore vanish, leaving terms of the form $\sin^{2l}(\theta)\cos^{2m}(\theta)$ ($l, m = [0, 1, 2, \ldots]$). It is readily shown that after the first few pulses, the remaining longitudinal magnetization M_z (z-component of $\mathbf{M}_{final}$) is as given in Table 1.

Many pulses. Observing that the sequence of values of M_z appears to converge, it is pertinent to investigate the behavior as n increases. Clearly, this matrix multiplication method becomes impractical for n much larger than tabulated here. An alternative method is to regard C as a composite rotation about its eigenvector **n.** After many rotations by all possible angles, only the component $\mathbf{v}$ of $\mathbf{M}_{init}$ parallel to $\mathbf{n}$ will remain, the perpendicular components having been completely dephased. We then take the average of $\mathbf{v}$ over all angles to arrive at the final magnetization. A suitably normalized eigenvector of C is

$$\mathbf{n} = \left(\frac{1}{\sqrt{1 + \sin^2\left(\frac{\theta}{2}\right)}}\right)\left(-\sin\left(\frac{\theta}{2}\right), \cos\left(\frac{\theta}{2}\right), \sin\left(\frac{\theta}{2}\right)\right), \quad [8]$$

and the component of $\mathbf{M}_{init}$ along this axis is

$$\mathbf{v} = (\mathbf{M}_{init}\cdot\mathbf{n})\mathbf{n} = M_0\left(\frac{\sin\left(\frac{\theta}{2}\right)}{1 + \sin^2\left(\frac{\theta}{2}\right)}\right)\left(-\sin\left(\frac{\theta}{2}\right), \cos\left(\frac{\theta}{2}\right), \sin\left(\frac{\theta}{2}\right)\right). \quad [9]$$

$\mathbf{M}_{final}$ is then given by $\alpha(-M_0, 0, M_0)$, where α is the mean value of

$$\frac{\sin^2\left(\frac{\theta}{2}\right)}{1 + \sin^2\left(\frac{\theta}{2}\right)}$$

which evaluates to $[1 - (\sqrt{2}/2)]$. This has a numerical value of 0.29.

ACKNOWLEDGMENTS

This work is funded in part by the Medical Research Council. The author is indebted to Dr. Timothy Spiller of Hewlett-Packard Laboratories (Bristol, UK) for the eigenvector analysis presented in the Appendix, and to Dr. Mark Bastin for useful discussions. One of the reviewers is to be thanked for highlighting the work of Mugler and Brookeman (*8*).

REFERENCES

1. G. T. Gullberg, M. A. Simons, and F. W. Wehrli, *Magn. Reson. Imaging* **6,** 437–461 (1988).
2. J.-H. Gao, S. K. Holland, and J. C. Gore, *Med. Phys.* **15,** 809–814 (1988).
3. J. C. Gatenby and J. C. Gore, *J. Magn. Reson. B,* **104,** 119–126 (1994).
4. T.-Q. Li, J. D. Seymour, R. L. Powell, K. L. McCarthy, L. Ödberg, and M. J. McCarthy, *Magn. Reson. Imaging* **12,** 923–934 (1994).
5. J. N. Oshinski, D. N. Ku, and R. I. Pettigrew, *Magn. Reson. Med.* **33,** 193–199 (1995).
6. G. Fürst, M. Hofer, M. Sitzer, T. Kahn, E. Müller, and U. Mödder, *J. Comput. Assist. Tomography* **19,** 692–699 (1995).
7. D. Atkinson and L. Teresi, *Magn. Reson. Quarterly* **10,** 149–172 (1994).
8. J. P. Mugler and J. R. Brookeman, *Magn. Reson. Med.* **23,** 201–214 (1992).
9. R. R. Edelman, H. P. Mattle, B. Walner, R. Bajakian, J. Kleefield, C. Kent, J. J. Skillman, J. B. Mendel, and D. J. Atkinson, *Radiology* **177,** 45–50 (1990).
10. D. S. Williams, J. A. Detre, J. S. Leigh, and A. P. Koretsky, *Proc. Natl. Acad. Sci. USA* **89,** 212–216 (1992).
11. J. A. Detre, J. S. Leigh, D. S. Williams, and A. P. Koretsky, *Magn. Reson. Med.* **23,** 37–45 (1992).
12. D. A. Roberts, J. A. Detre, L. Bolinger, E. K. Insko, and J. S. Leigh, *Proc. Natl. Acad. Sci. USA* **91,** 33–37 (1994).
13. O. T. Karlsen, J. H. N. Creyghton, A. F. Mehlkopf, and W. M. Bovee, Proceedings of the International Society for Magnetic Resonance in Medicine, Fourth Scientific Meeting, New York, p. 1308, 1996.
14. S. Francis, A. Freeman, P. Gowland, and R. Bowtell, Proceedings of the International Society for Magnetic Resonance in Medicine, Fifth Scientific Meeting, Vancouver, Canada, p. 83, 1997.
15. W. T. Dixon, L. N. Du, D. D. Faul, M. Gado, and S. Rossnick, *Magn. Reson. Med.* **3,** 454–462 (1986).
16. R. R. Edelman, B. Siewert, D. G. Darby, V. Thangaraj, A. C. Nobre, M. M. Mesulam, and S. Warach, *Radiology* **192,** 513–520 (1994).
17. S.-G. Kim, *Magn. Reson. Med.* **34,** 293–301 (1995).
18. K. K. Kwong, D. A. Chesler, R. M. Weisskoff, K. M. Donahue, T. L. Davis, L. Ostergaard, T. A. Campbell, and B. R. Rosen, *Magn. Reson. Med.* **34,** 878–887 (1995).
19. C. T. W. Moonen and P. C. M. van Zijl, *J. Magn. Reson.* **88,** 28–41 (1990).
20. G. J. Barker and T. H. Mareci, *J. Magn. Reson.* **83,** 11–28 (1989).
21. R. Gronas, P. G. Kalman, D. S. Kucey, and G. A. Wright, *J. Magn. Reson. Imaging* **7,** 637–643 (1997).
22. Y. Zur, M. L. Wood, and L. J. Neuringer, *Magn. Reson. Med.* **21,** 251–263 (1991).